IEEE Access
Multidisciplinary | Rapid Review | Open Access Journal

Received June 1, 2021, accepted June 12, 2021, date of publication June 16, 2021, date of current version June 23, 2021.

Digital Object Identifier 10.1109/ACCESS.2021.3089697

Design and Application of a Self-Powered Dual-Stage Circuit for Piezoelectric Energy Harvesting Systems

MAHESH EDLA[1], YEE YAN LIM[1], RICARDO VASQUEZ PADILLA[1], AND DEGUCHI MIKIO[2]
[1]School of Environment, Science and Engineering, Southern Cross University, East Lismore, NSW 2480, Australia
[2]Department of Electronics and Control Engineering, Niihama College, National Institute of Technology, Niihama 790-8570, Japan

Corresponding author: Mahesh Edla (mahesh.edla@scu.edu.au)

This work was supported in part by Southern Cross University, Lismore, NSW, Australia.

ABSTRACT This paper describes the design and practical application of a dual-stage H-Bridge (DSHBR) circuit to reduce the rectification losses and mitigate ripples in piezoelectric energy harvesting. The proposed DSHBR circuit integrates both AC-DC and DC-DC conversion processes using bidirectional switches and a step-up DC-DC converter, which applies to both positive and negative half cycles. One additional feature is that it does not require external power to turn on the bidirectional switches ($V_{th} < 0.3$ V). Such feature facilitates active rectification at very low AC voltages ($V_{ac} < 0.5$) generated by the piezoelectric device (PD). To validate the performance of the proposed circuit, a series of experimental tests were conducted. Firstly, the performance of circuit on rectifying the PD output was investigated using a shaker to generate high and low frequency excitations. Next, real-life testing was conducted with human arm motion as the source of excitation. Then, the ability of the entire system to charge solar batteries was investigated. The outcome shows that the DSHBR circuit prominently increased the rectified voltage and the output power while stabilising the DC voltage when compared with the conventional H-Bridge circuit.

INDEX TERMS Piezoelectric energy harvesting, self-powered H-Bridge circuit, dual-stage H-Bridge circuit, rectifier, solar battery.

I. INTRODUCTION

In recent years, human beings are witnessing a rapid increase in the usage of renewable energy sources (RES), such as solar [1], wind [2], thermal [3] and mechanical energy (ME) [4]. Such trend is encouraging as it reduces the reliance on non-renewable energy sources, particularly crude oil and fossil fuels. To utilise renewable energy, effective energy harvesting and conversion mechanisms are crucial. Lately, the emergence of mechanical vibration-based piezoelectric energy harvesting (PEH) technology as a sustainable, micro-scale energy harvesting and conversion system is found to be a potential alternative to conventional batteries with a limited life-span for powering electronic devices with low energy demand. Its applications include medical implant and wireless sensors for structural health monitoring [5], [6].

The ubiquity of ME from a wide range of sources, namely human, machinery, wind, roadway and aircraft, enables the PEH technology to be widely applicable. A flow chart, which demonstrates the process and applications of the PEH systems, is depicted within the context of Fig. 1. In this technology, the piezoelectric device (PD) generates electrical energy in the form of alternating current (AC) as a consequence of mechanical vibrations.

Yet, to power electronic devices or store the AC based energy for future use, it needs to be converted into direct current (DC) voltage. Thereby, an electronic circuit is required to perform such rectification efficiently. Over the years, various rectifier circuits have been proposed by the research community. They are reviewed in the following paragraphs.

The simplest way to convert AC into DC is by using an full-wave bridge rectifier (FBR) circuit [7]–[15]. This circuit suffers from various shortcomings, despite its simplicity and popularity. The key shortcomings include:

1. In the most commonly used FBR circuit, the PD voltage, V_{PD} must be higher than the conventional diode's forward voltage, V_f (i.e. $V_{PD} > 0.72\ V_f$) [16] to convert AC

The associate editor coordinating the review of this manuscript and approving it for publication was Yuh-Shyan Hwang.

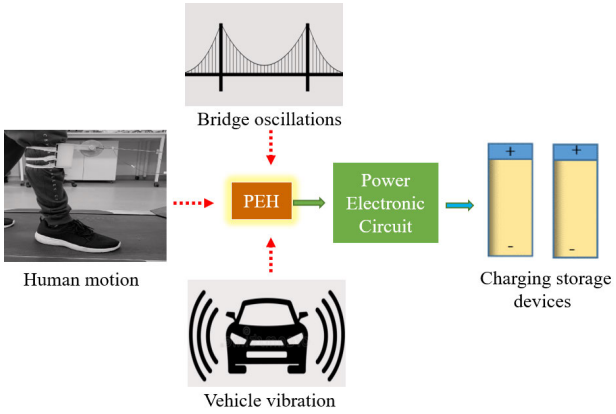

FIGURE 1. Application of PEH systems.

into DC, which renders the FBR circuit inefficient (suffers from rectification losses) and unsuitable for many applications with low voltage.

2. The rectified voltage, V_{dc} converted by the FBR circuit, is unstable due to the presence of ripples.

To overcome the abovementioned drawbacks (i.e. high forward voltage and unstable rectified voltage), various linear and non-linear electronic circuits have been proposed. One example is the diode-less rectification circuit proposed by [17], as shown in Fig. 2. Its design incorporated bidirectional transistors to attenuate the forward voltage losses in the rectification process. However, the study did not present the output power extracted from the circuit.

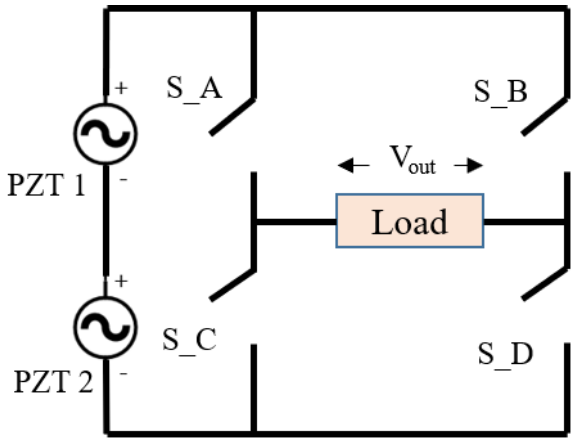

FIGURE 2. The diode-less rectifier circuit.

In addition, no comparison has been made with conventional circuits or existing literature. Practical application and appropriate mechanical and electrical boundary conditions were not considered. Its effectiveness is unknown.

A metal oxide semiconductor field effect transistor (MOSFET) circuit was proposed by [18] to mitigate the conversion losses in the rectification process due to the forward voltage of diode. A key shortcoming of their proposed circuit is the need of an external power supply to turn on the MOSFETs, which is adamant and unrealistic in real-life applications. Another study on the MOSFET based rectification process was recently conducted by [19] to decrease the power consumption of the circuit. An improvement in output power and efficiency was augmented in comparison with the FBR circuit. Nevertheless, due to high threshold voltage, V_{th} of MOSFET devices, the power conversion from the PD was limited. The stability of the output waveform was not discussed in the study.

To expel this shortcoming, a MOSFET dependent rectifier circuit was proposed in [20]. Using the proposed rectification method, a significant improvement in power conversion was congregated. However, the proposed circuit integrated a switching tactic that required extra electronic components, such as a large inductor and the use of pulse with modulation (PWM) technique, which rendered the circuit complex and costly. This proposed study did not present the extracted output power. Practical application and appropriate electrical boundary conditions were not presented.

Kirubaveni Savarimuthu [21] proposed a dual-stage PEH circuit to reduce the voltage drop in the rectification process. At its resonance frequency of 21.4 Hz, the proposed circuit generated the highest power, approximately 66 mW. This circuit could be turned on with a very low voltage (500 mV). The output of PD was rectified and boosted by 70.03 % with minimal losses. In their study, the performance of PD and single stage conditioning circuit has been analysed. However, the proposed circuit required an external power supply to operate the switching process, which was not practical.

Another dual-stage rectifier circuit was proposed by [22]. The proposed controller varied the switching frequency, f_s of the step-down converter circuit to maximise the output power flow into the battery. However, due to its switching frequency, the switching losses were higher than the output power.

An energy-harvesting circuit with clock booster for PEH application was approached by [23] to attenuate the voltage drop in the rectification process. The proposed circuit included a clock booster to maximise the amplitude of the pulses and to turn on the buck-boost converter. It is thus also known as the second stage converter. This circuit was constructed with CMOS technology and was tested through simulation. It was found that the output voltage was nearly 0.8 V_{dc} at 100 kHz with an input voltage of 1.6 V_{ac}. Additional components were required in the circuit, the rectified voltage was also limited and unstable.

A recent study by the authors (Edla *et al.* [12]) modified the abovementioned MOSFET bridge rectifier circuit to a self-powered H-Bridge circuit. The proposed circuit was successfully applied to ultra-low voltage and high frequency application. The outcome showed that the proposed circuit notably increased the output voltage and output power compared with the conventional FBR circuit. The ripples in the rectified voltage waveform were also comparatively less. However, the issue of ripples in the output voltage was not investigated in detail. Later, an improved rectifier circuit for PEH from human motion was proposed by the

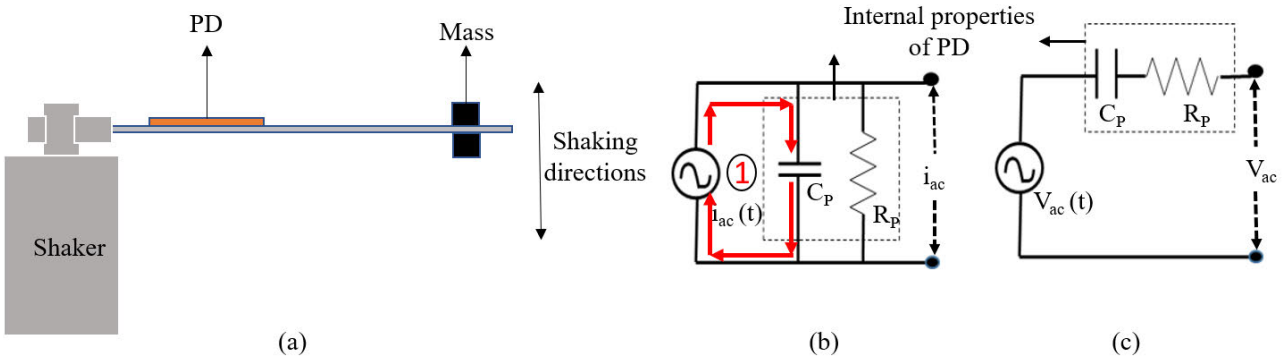

FIGURE 3. (a) A PD excited by a shaker, (b) PD as a current source, (c) PD as a voltage source.

authors (Edla *et al.* [13]). The proposed rectifier circuit was successfully applied to low frequency vibration. A series of experimental tests were conducted, with three sources of low-frequency vibrations, namely mechanical shaker, human performing walking motions and cycling motions. The results showed that their proposed circuit notably increased the voltage and power produced from the PD in comparison with the conventional FBR circuit. Similarly, the problem of ripples in rectified voltage remained unresolved.

As identified in the literature, most researchers focused on increasing the maximum output power from the PD to the load. However, thus far, very few studies have considered the method of reducing conversion losses in the rectification process. In addition, the issue of ripples in the rectified voltage waveform was not addressed. Therefore, there is a need to design an electronic circuit to bridge the above-mentioned literature gap associated with the mechanical and electronics interface. This is attempted in this study with the proposition of a self-powered dual-stage H-Bridge (DSHBR) circuit. This proposed circuit is an improved version of the self-powered H-Bridge circuit, previously proposed by the authors [12], [13]. The key difference between the previous H-Bridge circuit and the currently proposed circuit is that the H-Bridge circuit is single stage, which only converts AC-DC, while the proposed DSHBR includes two stages (Stage 1: AC-DC conversion with reduced conversion/rectification losses, Stage 2: DC-DC conversion with rectified voltage stabilisation). Other key advantages of the proposed circuit over the existing circuits available in the literature are as follows:

1. The proposed circuit does not require additional components such as polarity detectors nor external power supply to turn on the MOSFETs at any stages.
2. It also does not require external power supply to turn the DC-DC converter ON. Therefore, maintenance is not required, rendering the PEH system conveniently applicable to various environments, regardless of the amplitude of ambient vibrations.
3. It works at very low voltage ($< 0.5\ V_{ac}$), which is not possible with conventional FBR circuit.
4. The cost is low as components used are minimal.

A detailed explanation of the proposed circuit is outlined in the following sections. Experimental tests were designed and performed to investigate the performance of the circuit. Both controlled, laboratory-based experiment and real-life test on human arm were conducted. The feasibility of using the output power to charge a solar battery was also studied.

II. PEH CIRCUITS

In this section, the internal characteristics of a mechanically excited PD used in the PEH system are explained. The conventional FBR circuit and the proposed DSHBR circuit are then delineated.

A. INTERNAL CIRCUIT OF PD

When the PD is subjected to excitation, such as by a mechanical shaker (Fig. 3a), it can be modelled as a current source, i_{ac} (Fig. 3b) or a voltage source, V_{ac} (Fig. 3c) in parallel and series with its internal capacitance, C_P and resistance, R_P, respectively.

The AC voltage generated by the PD includes positive and negative half cycles. The generated voltage needs to first charge its internal capacitor (Figs 3b and c). As a result, the voltage and current waveforms of the PD vary with the mechanical excitations, as shown in Fig. 4. As depicted in Fig. 4, the effectiveness of the PD is closely related to the duration of Intervals 1 and 2. During Interval 1 from time t_0 to t_1, the generated current charges its internal capacitor. As a result, there is no output through the PD, so the load capacitor CL is not charged. This state continues until Interval 2, where the magnitude of the PD voltage, V_{ac} and load capacitor voltage is equal. At this interval, from time t_1 to t_2, the load capacitor is charged. A similar process occurs in the negative half cycle from time t_2 to t_3 and t_3 to t_π. The current generated by the PD can be stated as:

$$i_{ac}(t) = \widehat{I_{ac}} \sin(\omega t) \tag{1}$$

where $\widehat{I_{ac}}$ is the magnitude of current, ω is the angular frequency, and t is time.

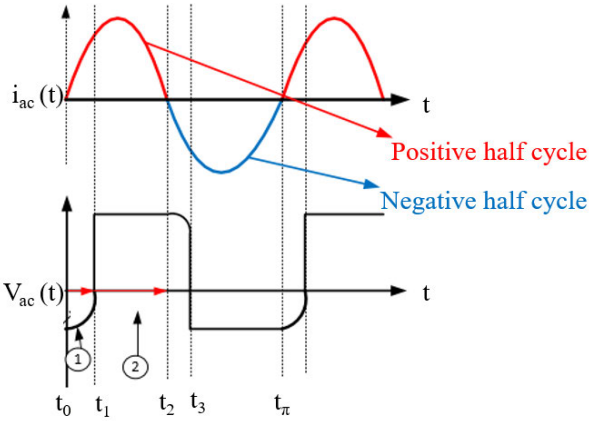

FIGURE 4. The waveforms of current and voltage of a vibrating PD.

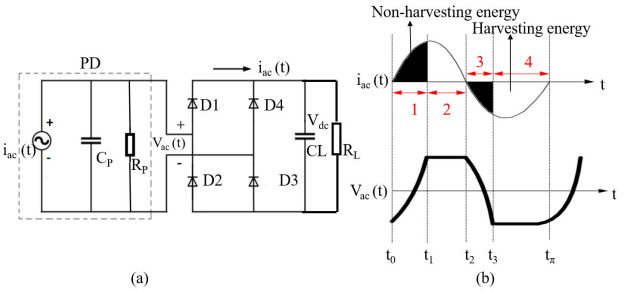

FIGURE 5. (a) Conventional FBR circuit and, (b) typical current and voltage waveforms generated by the PD.

B. CONVENTIONAL FBR CIRCUIT

A conventional FBR circuit and its corresponding voltage and current waveforms are shown in Fig. 5. When the generated PD voltage is less than the rectified voltage, $V_{dc} + 2\ V_d$ (where V_d is the voltage drop across diode), the FBR circuit is blocked, and the load capacitor is not charged. This period is known as non-harvesting energy period (Interval 1 and 3 in Fig 5b). When the PD voltage is equal to the rectified voltage, $V_{dc} + 2\ V_d$, the FBR circuit starts to conduct, and the load capacitor is charged. This period is known as harvesting energy period (Interval 2 and 4). Further explanations of the FBR circuit's operation can be found in [12].

When the diodes are in the conduction state in both half cycles, the output current flows into the load capacitor. As a result, the load capacitor reaches its peak value. Then, the load capacitor, CL discharges through the load resistance, R_L. In other words, the load resistor takes some current from the load capacitor. The charging and discharging of the load capacitor results in instability of the rectified voltage, which is denoted as a ripple voltage. Fig. 6 shows the rectified voltage waveform, V_{dc} produced by FBR circuit in PEH, which contains ripples. When the load capacitor is connected in parallel with the FBR circuit (i.e. connected to the above-mentioned waveform), the rectified voltage is limited to the load capacitor rating [24], [25]. The output power varies with the rectified voltage, and the peak output power [26] occurs when:

$$V_{dc} = \frac{I_{ac}(t)}{2\omega C_P} \tag{2}$$

Besides the total charge produced by the PD in both positive and negative half cycle, Q_{total} can be stated as follows:

$$Q_{total} = 2C_P V_{ac}(t) \tag{3}$$

C. DUAL-STAGE H-BRIDGE RECTIFIER CIRCUIT

In this study, a DSHBR circuit is proposed to reduce rectification losses, operate at low AC voltages, and mitigate the ripples in output voltage. The proposed circuit is illustrated in Fig. 7. It is designed to operate across two stages. Stage – 1 involves the operation of a self-powered H-Bridge circuit for rectifying AC voltage to DC voltage, while Stage – 2 involves the DC-DC converter for stabilising the rectified voltage. Note that one distinct advantage of the proposed DSHBR circuit is that it does not require an external power supply at any stage to turn on the bidirectional switches, i.e. the MOSFET. The proposed circuit can potentially be used with the PEH system to harness vibration from a wide range of sources. In the following paragraphs, the mode of operation, key features and benefits of the circuit at both stages are explained.

1) STAGE – 1

The H-Bridge circuit (Stage – 1) differs from the conventional FBR circuit in which it comprises four MOSFETs instead of four diodes in the latter. The advantage of MOSFET is that the D to S voltage can be adjusted by the PD voltage, which is applied across the G terminal. Besides, the MOSFET allows a bi-directional flow of current (D $\leftrightarrow$ S), while diode only allows current in one direction. Operation wise, the DSHBR circuit undergoes four modes of operation at Stage - 1, over the positive and negative half cycles. The processes involved in Stage – 1 operation of the circuit [12] are summarised in Table. 1. When the rectified voltage is stored in the load capacitor, CL1, Stage – 2 of the dual-stage circuit begins to operate.

2) STAGE – 2

The load capacitor, CL1 (charged during Stage - 1) in Fig. 7, is chosen to be large enough to capture a small amount of power generated from low amplitude vibrations. Subsequently, the capacitor has a much lower voltage than a standard electrolytic capacitor and requires a longer charging period. Therefore, a Zener diode (D1) is connected in parallel with CL1 to prevent the voltage across CL1 from exceeding its peak voltage rating. CL1 then discharges to load resistor, R_L.

As mentioned, this DC-DC converter is able to maintain a fixed and stable rectified voltage at the output terminal. It includes a synchronous rectification process, which eliminates the need of diodes, minimises the size of the circuit and improves the overall efficiency. A detailed explanation of the

TABLE 1. Stage - 1 operation of DSHBR circuit in both positive and negative half cycles.

Circuit	Positive half cycle		Negative half cycle	
	Mode 1	Mode 2	Mode 3	Mode 4
Stage - 1 of DSHBR	When $t_0 < t \leq t_1$ • Interval 1 begins • MOSFETs: OFF • CL1: Not charging	When $t_1 < t \leq t_2$ • Interval 2 begins • MOSFET 1, 4: ON • CL1: Charging	When $t_2 < t \leq t_3$ • Interval 3 begins • MOSFETs: OFF • CL1: Not charging	When $t_3 < t \leq t_4$ • Interval 4 begins • MOSFET 2, 3: ON • CL1: Charging

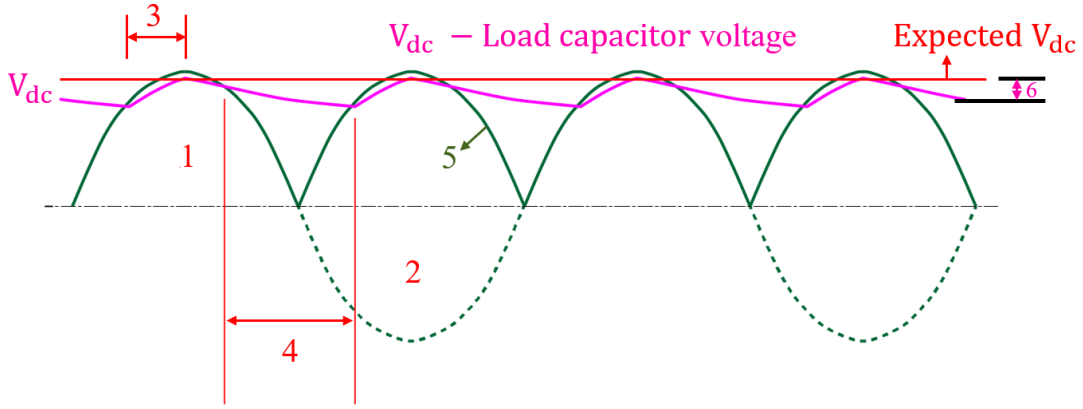

1. Positive half cycle, 2. Negative half cycle, 3. Charging time, 4. Discharging time, 5. Rectified voltage, 6. Ripple voltage

FIGURE 6. Rectified voltage waveform by FBR circuit with ripples.

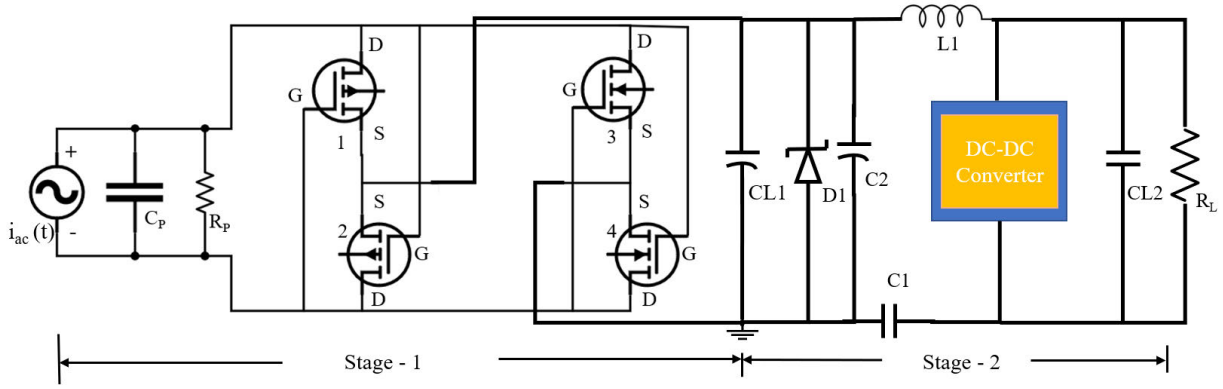

FIGURE 7. The proposed DSHBR circuit with MOSFETs. (1: PMOS, 2: PMOS, 3: NMOS, 4: NMOS, G: Gate, D: Drain, S: Source).

synchronisation process of DC-DC converter is stated in [27]. The stabilised DC voltage through the DC-DC converter is eventually stored in the load capacitor, CL2. One additional benefit of the proposed circuit is that if the voltage of load capacitor, CL1 drops below the minimum voltage of operation, the circuit continues to provide stable output voltage, as long as the voltage of CL1 is not lower than the power limit of the DC-DC converter.

At this stage, a DC-DC converter, namely Maxim 1675 [27] is adopted to stabilise the rectified voltage without using switching methods, inductors in the range of milli-Henry, diodes, and pulse with modulation methods. The adopted converter carries two functions: (1) for low to high voltage conversion and (2) for DC voltage stabilisation. As a result, the adopted DC-DC converter reduces power dissipation, cost and maintenance.

Note that Stage – 2 also does not require any additional power supply to turn the DC-DC converter operation ON. Therefore, it does not require logic gates, switching pulses and additional ICs [28] to operate switches in the dual-stage

conversion. Further, as identified in [21], [29], [30], the switching frequency results in higher power dissipation in the circuit and requires regular maintenance.

The magnitude of extracted output power is a useful indicator of the performance of the proposed DSHBR circuit. In this study, the rectified voltage and the output power are used to compare the performance of the proposed circuit with other previously proposed circuits in the literature. The input power, P_{ac} can be expressed as [31]:

$$P_{ac} = \frac{V_{Pk}}{\sqrt{2}} . \frac{I_{Pk}}{\sqrt{2}} \cos\varphi \tag{4}$$

where V_{Pk}, I_{Pk} are the peak voltage, current, and φ is the phase angle between the voltage and the current of PD.

Considering the rectified DC voltage and the current are generally constant, the output power of the DSHBR circuit, P_{out} can be calculated through the product of voltage across the load capacitor, V_{CL2} and the current, I_{CL2} through it [20]:

$$P_{out} = V_{CL2^*} I_{CL2} \tag{5}$$

As stated in [13], the MOSFETs parasitic capacitance between the terminals affects the performance of the Stage – 1 circuit (i.e. H-Bridge), in particular, the power. Power loss, $P_{switching\ loss}$ in the MOSFET occurs during the switching process, known as the switching losses in H-Bridge circuit, which can be stated as [12], [32]:

$$P_{switching\ loss} = \frac{1}{2} V_{DS}\, I_D\, f_s (t_{on} + t_{off}) \tag{6}$$

where t_{on} and t_{off} refer to the turn on and turn off time of the MOSFETs, respectively.

The total power loss of the proposed circuit can be calculated as follows:

$$P_{Loss} = P_{ac} - P_{dc} \tag{7}$$

where P_{Loss} refers to total power loss, while P_{ac}, P_{dc} refer to input power and output power of the proposed circuit, respectively.

III. EXPERIMENTAL STUDY

In this study, the performance and applicability of the proposed DSHBR circuit for PEH was experimentally studied using two test setups based on two different sources of mechanical vibrations, namely shaker-induced vibration (SIV) and human motion-induced vibrations (HMIV).

In the SIV test, the performance of the proposed circuit was tested at low and high frequency generated by the mechanical shaker. Application-wise, the output power was used to charge a solar battery. The SIV test was first conducted to better understand the performance of the proposed circuit for rectification and stabilisation of AC voltage under controlled mechanical excitation before the more erratic HMIV were investigated. In the HMIV test, rectification and stabilisation of AC voltage harvested from low frequency human motion was investigated. Charging of small storage devices, namely capacitors, were attempted.

Overall, four experimental tests were conducted, the energy sources of Tests 1, 2 and 3 were SIV, whereas Test 4 was HMIV. In Test 1, the output power extracted from PD (Microfibre composites, MFC) through the DSHBR was investigated at high frequency (100 Hz) by varying the input voltage. Test 2 was similar to Test 1, but the excitation frequency was much lower (2, 5, and 10 Hz) to simulate human motion [4], [33]. As the PD voltage is more erratic at low frequency, Test 2 was also compared with the previously published results using H-Bridge circuit [13]. In Test 3, the DSHBR was used to charge a solar battery with an input voltage of 3 V_{ac} at a frequency of 5 Hz and 10 Hz. In Test 4, the source of vibration was a moving human arm at varying angle, and the type of PD used was Polyvinylidene Fluoride film (PVDF).

In all four test scenarios, the voltage generated by the PD was rectified by the DSHBR circuit, and stored in a load capacitor, CL2. A range of resistances R1, R2, R3 and R4, were sequentially connected for each case. Finally, the output power of the proposed circuit was calculated using Eq. 5. A summary of Tests 1 – 4 and the components used in DSHBR circuit are tabulated in Table 2 and 3, respectively.

A. EXPERIMENTAL SETUP

1) SIV TEST (TEST 1-3)

In the SIV test, an MFC patch (Model: M2814 - P2, Dimension: 37 mm × 17 mm × 0.180 mm, Capacitance: 30.79 nF) was used as PD in Test 1, 2, and 3. The MFC patch was attached to the surface of one end of an aluminium cantilever beam (dimension: 205 mm X 20 mm X 1 mm). Two permanent magnets were attached to the other end of the cantilever beam as proof mass, as shown in Fig. 8. The threshold voltage of the MOSFETs was verified with a voltmeter (FLUKE 115).

The output voltage and the current were measured by the voltmeter and an ammeter (CD 771). Besides, the rectified voltage waveform was also observed in an oscilloscope (TBS 1052B). Fig. 8 shows the experimental setup for the SIV test. A function generator (Agilent 33210A) was used to deliver a sinusoidal signal to a power amplifier (2706, B & K Agilent), which then amplified the signal before activating the mechanical shaker (APS – 113). The mechanical shaker generated harmonic vibrations according to the input frequency and amplitude to excite the cantilever beam with attached PD. Note that in all testing scenarios, the amplitude and frequency of the PD were adjusted by the amplifier and function generator, respectively. In other words, the input voltage applied to the DSHBR circuit was adjusted at each frequency by using an amplifier. Note that when the current produced by the PD at each frequency varied, the input power to the DSHBR circuit also varied [12]. When the input voltage was applied to the DSHBR circuit, it conducted the operation at both Stage – 1 (AC-DC conversion) and Stage – 2 (DC-DC conversion).

TABLE 2. Summary of test scenarios for DSHBR.

Sources of Excitation	Test scenarios	Frequency (Hz)	Input voltage (V_{ac})	Types of PD	Load capacitors (μF)	Load resistors (kΩ)
Shaker	Test 1	100	0.5, 0.7, 1.0, 1.25	MFC	10	R1 = 100, R2 = 330, R3 = 660, R4 = 920
	Test 2	2, 5, 10	2, 5, 10			
	Test 3	5, 10	3		Solar battery, 1.2 V_{dc}, 4 mA	100
Human motion	Test 4	Angle between upper arm and forearm (^{0}) 0, 30, 45, 60, 90		PVDF	10	100

TABLE 3. List of components used in DSHBR circuit.

Stages	Components	Parameters
1	PMOS – RZR040P01	0.3 V_{th}, 20 V
	NMOS – AP2306AGN	0.3 V_{th}, 20 V
2	Inductor	22 μH

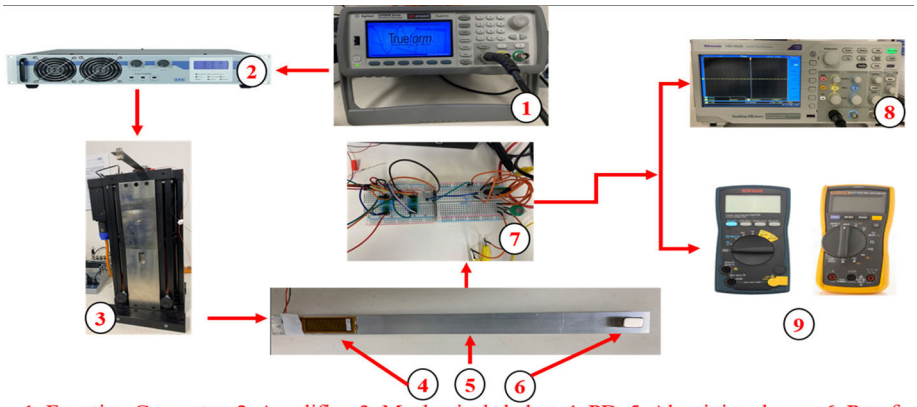

FIGURE 8. Experimental setup of SIV test.

2) HMIV TEST (TEST 4)

The experimental setup of the HMIV test is presented in Fig. 9. In this configuration, the proposed circuit was tested with HMIV as a source of excitation. Typical human's arm movement, as shown in Fig. 10, was performed. The movement of the arm was defined by the relative angles between the upper arm and forearm, between 0 – 90 degrees. The power generated at five distinct angles (tolerance ±5 degrees) was measured and recorded.

For this test (Test 4), a distinct type of PD, namely PVDF, was adopted and patched on a human's left hand. The PVDF was patched at the elbow, where the highest strain was expected to occur, as shown in Fig. 9. Note that unlike Test 1, 2 and 3, the amplitude and frequency of Test 4 was not controlled.

Similar to previous tests, the electricity generated by the PVDF as a result of arm motion was sent to the proposed DSHBR circuit for rectification and stabilisation. The ensuing output voltage and current were displayed and recorded through the oscilloscope.

IV. RESULTS AND DISCUSSIONS

A. TEST 1 (SIV, HIGH FREQUENCY)

The rectified voltage and output power acquired from Test 1 are described within the context of Figs. 11 (a) and (b). The rectified voltage and output power through the proposed circuit with varying input voltage (0.5 – 1.25 V_{ac}) and loads (100 – 920 kΩ) are compared.

From Fig. 11(a), it can be noticed that when the input voltage (V_{ac}) increased from 0.5 – 1.25 V_{ac}, the voltage (V_{dc}) rectified through DSHBR circuit increased accordingly. The increasing trend of rectified voltage is consistent with all resistances.

Initially, 0.5 V_{ac} was applied to the DSHBR circuit. As mentioned in Table. 1, when the threshold voltage of MOSFETs in DSHBR was less than the input voltage (Stage – 1), the AC voltage was converted into DC voltage, which was then stored in the load capacitor, CL1. Then, the DC-DC converter operation (Stage – 2), which included the synchronous rectification process, occurred by turning on the inbuilt MOSFETs in the DC-DC converter. An inductor

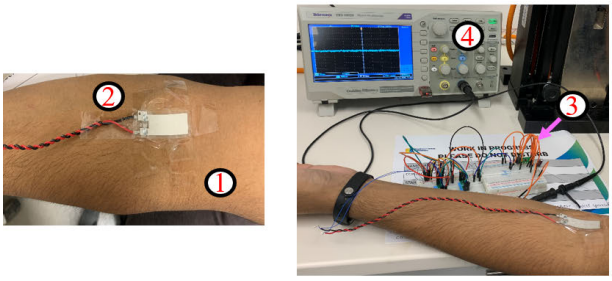

1) Human hand, 2) PVDF, 3) DSHBR circuit, 4) Oscilloscope

FIGURE 9. Experimental setup of Test 4.

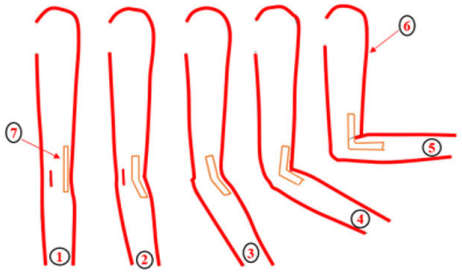

1. 0 degrees, 2. 30 degrees, 3. 45 degrees,
4. 60 degrees, 5. 90 degrees, 6. Human arm, 7. PVDF

FIGURE 10. Testing scenarios of HMIV.

that was in series with CL1 stored the current delivered by CL1. Considering the inductor has DC resistance that effectively lowered the efficiency, a smaller inductor was intentionally chosen to mitigate the negative effect. The output of the converter, which was the stabilised rectified voltage, was eventually stored in CL2. The process was similar for other input voltages. Note that ripples were observed in the output voltage waveform due to a higher peak in inductor currents.

It is worth emphasising that the resistance path of MOSFET from drain to source can be adjusted by varying the applied voltage at the gate terminal, as depicted in Fig. 11(a). When 0.5 V_{ac} was applied to the DSHBR circuit, 0.25 V_{dc} of rectified voltage was produced and stored in CL2. On the other hand, when 1.25 V_{ac} was applied, the voltage rectified and stored in CL2 increased approximately in a linear manner. At this instance, it can be noticed that the resistance path from D-S in the MOSFET was reduced. Therefore, the rectified voltage increased with increasing input voltages from 0.5 to 1.25 V_{ac}. When the input voltage on gate terminal was positive, say 0.5 V_{ac} with respect to the source, an electric field was established between the drain and the source (Fig. 7). Eventually, negative charges induced in P-substrate formed p-layer below the gate terminal, causing the p-layer to change to an induced n-layer. These charges (i.e. electrons) formed n- channel between two n+ regions (one n+ region on drain, the other n+ region on source), which caused current to flow from drain to source.

When the applied gate voltage was high, i.e. 1.25 V_{ac} (Fig. 11), the induced n- channel became deeper and more current flowed from drain to source. This showed that the gradual increase of gate voltage enhanced the drain to source current. Consequently, when the applied PD voltage was increasing from 0.5 – 1.25 V_{ac}, the rectified voltage also increased accordingly. In all scenarios, the rectified voltage was measured from CL2.

Next, the output power was calculated using Eq. 6, and the relationship between the input voltage and the output power at a frequency of 100 Hz is shown in Fig. 11(b). Highest output power was generated and stored in CL2 with an input voltage of 1.2 V_{ac}, while lowest power was observed with input voltage of 0.5 V_{ac} with load resistance, R4.

Another observation was that the rectified voltage increased with increasing load resistances. This trend was consistent across all input voltages and agreed well with Ohms' law. On the other hand, contrary to the rectified voltage, the trend of output power (Fig. 11b) with resistance was different. The reason for delivering different output power at different resistance was that the current through different resistors was different. As a result, the calculated output power was also different.

The outcome of Test 1 (Fig. 11) demonstrated the successful application of the proposed DSHBR circuit in converting AC voltage from PD into DC voltage by using low threshold voltage MOSFETs, which eliminated the forward voltage losses, and subsequently stored in a storage device. The proposed circuit was capable of converting AC into DC with an input voltage as low as 0.5 V_{ac}, which was lower than the forward voltage of diode. This outcome satisfied the first objective of this study, which is to convert AC into DC by eliminating the forward voltage losses. In Test 2, 3, and 4, the issue with unstable PD voltage at low frequency [4], [12] will be addressed.

B. TEST 2 (SIV, LOW FREQUENCY)

In Test-2, the performance of DSHBR was tested at low frequency (i.e. 2, 5 and 10 Hz). At each frequency, three different input voltages, 2, 5 and 10 V_{ac} were applied, sequentially. Then the rectified voltage was stored in CL2 with varying load resistance. The test details were tabulated in Table 1. At such low frequency, fluctuation of the input voltage waveform was more pronounced than Test 1.

The voltage waveforms captured from the oscilloscope at three frequencies with an input voltage of 5 V_{ac} are shown in Fig. 12 for illustration; other experimental results of Test 2 are summarised in Table 4.

Note that for all frequencies adopted in Test 2, the voltage rectified by the proposed DSHBR circuit showed a similar trend as in Test 1 (i.e. output voltage increased with an increase in input voltage). From Fig. 12, it can be noticed that, in the case of 2 Hz and 5 Hz, most of the ripples in the voltage waveform rectified by the DSHBR were eliminated. Yet, some ripples remained to be seen at 10 Hz due to a higher frequency of excitation.

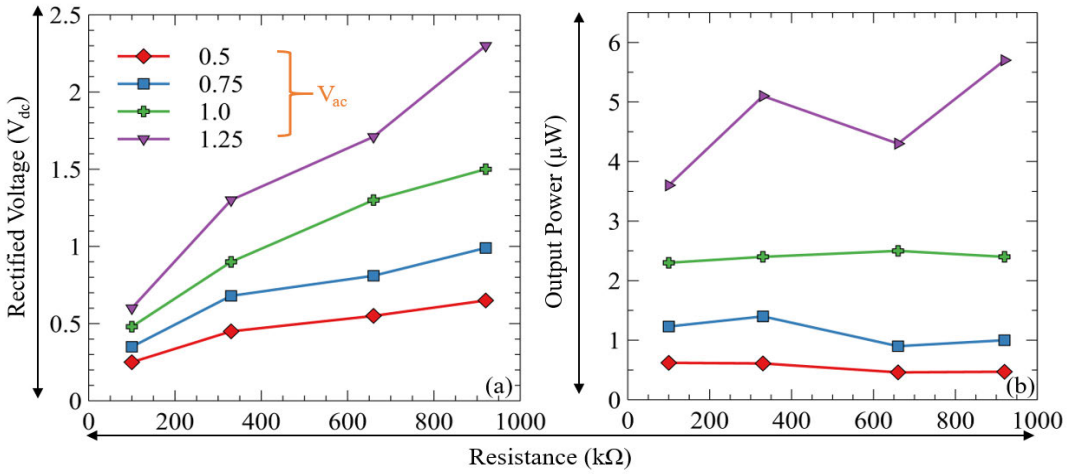

FIGURE 11. Rectified voltage and output power versus various resistances at 100 Hz.

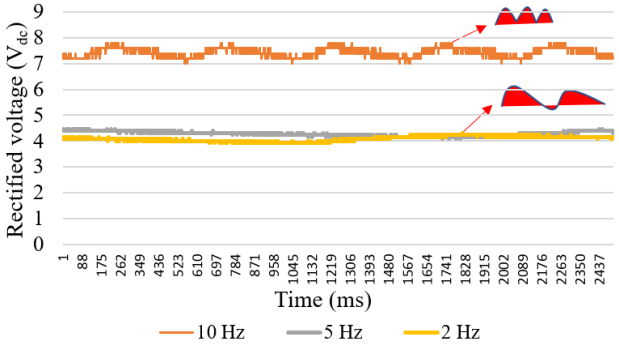

FIGURE 12. The waveforms of rectified voltage through DSHBR circuit at different frequencies with input voltage of 5 V_{ac}.

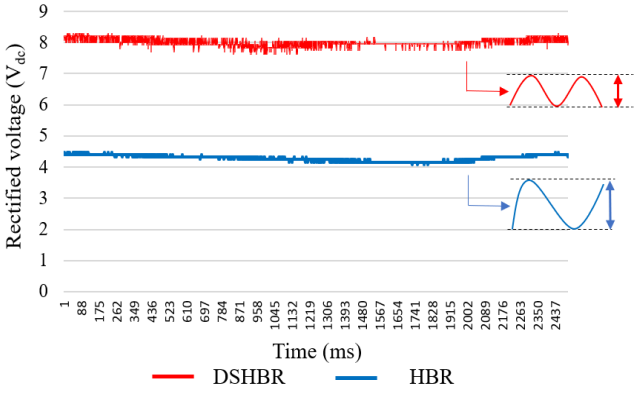

FIGURE 13. Comparison of voltage waveforms rectified by DSHBR and H-Bridge.

For the sake of comparison, the waveform rectified by DSHBR was compared with those rectified by an H-Bridge circuit recently studied by the authors (Edla *et al.* [12]), as shown in Fig. 13.

For a fair comparison, the same testing scenario (frequency of 2 Hz and input voltage of 5 V_{ac}) was applied to both circuits. Note that the H-Bridge circuit possessed only the AC-DC conversion circuit. The load capacitor, CL1, was charged by the H-Bridge circuit, then it was discharged by the load resistor. Thus, more ripples were observed in the voltage waveform rectified by the H-Bridge circuit. In the case of the DSHBR circuit, which possessed both AC-DC conversion and DC-DC conversion, the ripples in the load capacitor, CL1 of H-Bridge circuit, were reduced by the DC-DC conversion process before being stored in CL2.

Another observation from Fig. 13 is that under the same input condition, the voltage rectified by the DSHBR (7.9 - 8.2 V_{dc}) was significantly higher than the H-Bridge circuit (3.9 - 4.6 V_{dc}). This is due to the fact that the DC-DC converter in DSHBR also worked as a step-up converter.

As a result, it is evident that the proposed DSHBR circuit outperformed the conventional H-Bridge circuit in terms of magnitude and stability of the rectified voltage. The second intention of this study (i.e. to reduce the ripples in the rectified voltage) was demonstrated in Test 2.

C. TEST 3 (SIV, APPLICATION: SOLAR BATTERY Charging)

To demonstrate the practical applicability of the proposed DSHBR circuit, the power produced through the circuit was used to charge a solar battery (1.2 V, 4 mA battery), which is commonly used in solar garden lights. Under similar experimental conditions of Test 1 and Test 2 (Fig. 8), the solar battery was charged at a frequency of 5 Hz and 10 Hz with an input voltage of 5 V_{ac}.

At the frequency of 10 Hz, the solar battery was charged in 25 minutes. While at the frequency of 5 Hz, 35-36 minutes was required to charge to the same level. Note that with same input voltage, the input power is expected to be higher at higher excitation frequency. For the sake of comparison,

TABLE 4. Rectified voltage and output power through the proposed circuit in Test 1, 2 and 4.

Testing scenario	Frequency (Hz)	Input voltage (V_{ac})	Rectified voltage (V_{dc})				Output power (μW)			
			Resistance (kΩ)							
			100	*330*	*660*	*920*	*100*	*330*	*660*	*920*
Test 1	100	0.5	0.25	0.45	0.55	0.65	0.62	0.61	0.46	0.47
		0.7	0.35	0.68	0.81	0.99	1.23	1.4	0.9	1
		1.0	0.48	0.9	1.3	1.5	2.3	2.4	2.5	2.4
		1.25	0.6	1.3	1.71	2.3	3.6	5.1	4.3	5.7
Test 2	2	2	0.28	0.78	0.98	1.6	0.4	1.8	1.4	2.7
		5	0.9	1.9	2.9	4.5	8.1	10.9	12.7	22
		10	0.9	1.9	2.9	4.5	19.6	43.7	52.7	74.9
	5	2	0.22	0.6	0.98	1.6	0.4	1	1.4	2.8
		5	0.41	1.7	3.1	4.2	1.7	8.8	14.05	19.1
		10	1.41	2.9	5.8	8.3	19.9	25.4	50.9	75.5
	10	2	0.3	0.5	0.9	1.3	0.9	0.7	1.2	1.85
		5	0.43	1.3	3.5	7.6	1.9	5.2	19	62
		10	2.1	3.2	5.9	8.8	44.1	31.1	52.7	84.2

TABLE 5. Rectified voltage and output power through the proposed circuit in Test 4.

Testing scenario	Angle (^{0})	Resistance (kΩ)	Rectified voltage (V_{dc})	Output power (μW)
Test 4	0	100	0	0
	30		0.15	0.25
	45		1.7	28.9
	60		2.7	72.9
	90		3.4	115.6

a 1 cm × 1.5 cm solar panel with a DC-DC converter circuit typically charges the same solar battery in 4 - 5 hours.

D. TEST 4 (HMIV)

Referring to Fig. 9 and Fig. 10 for the HMIV experimental setup of Test 4, the angles of arm movement considered were 0, 30, 45, 60, and 90-degrees.

The AC voltage generated by the PVDF at different angles was applied to the proposed DSHBR circuit, and then the rectified voltage was stored in the load capacitor, CL2. The results are shown in Fig. 14. It can be seen that when the angle was less than 30 degrees, the rectified was very low. At 45 degrees, the rectified voltage was 1.6 V_{dc}. The voltage then increased progressively with increase in angles of movement. It can be identified that the rectified voltage has a positive correlation with the angle of the arm, which affected the bending angle of the PVDF. The reason being, higher strain was experienced by the PVDF at a larger angle. Higher voltage was subsequently generated. The highest voltage was thus achieved at 90 degrees (largest angle).

Similar to Test 1 and Test 2, the voltage rectified through the DSHBR circuit was directly proportional to the input voltage. The corresponding output power was also calculated and tabulated in Table 5. The outcome demonstrated the versatility of the proposed DSHBR circuit, as it was also applicable to very low frequency human movement (in this case, quasi static) with high strain. Thus, it was concluded that the proposed DSHBR circuit performed satisfactorily with low and high frequency of excitations, which was usually unachievable by other types of rectifier circuit [34].

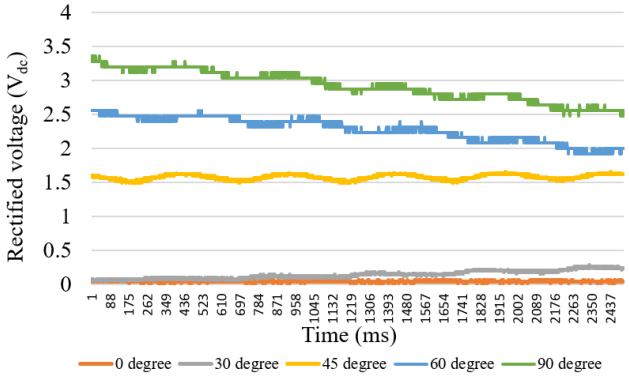

FIGURE 14. The voltage rectified by DSHBR at different angles of arm movement.

E. RECTIFIED VOLTAGE AND OUTPUT POWER THROUGH DSHBR CIRCUIT IN TESTS 1, 2 AND 4

The rectified voltage and output power through the proposed DSHBR circuit at different frequency and resistance in Tests 1, 2 and 4 are summarised in Tables 4 and 5. From Table 4, it can be noticed that the highest voltage rectified by the proposed DSHBR circuit was 2.3 V_{dc} and the corresponding output power was 5.7 μW with an input voltage of 1.25 V_{ac} at a frequency of 100 Hz (i.e. Test 1).

As stated in [34], the MOSFETs circuit did not work efficiently at low frequency due to its junction bias. This shortcoming was overcome in this study based on the experimental results as shown in Table 4 (Test 2), whereby regardless of frequency, the proposed circuit was able to rectify the

input voltage. For example, the highest rectified voltage and output power achieved were 4.5 V_{dc} and 74.9 μW, 8.3 V_{dc} and 75.5 μW, and 8.8 V_{dc} and 84.2 μW, when 10 V_{ac} was applied at different low frequencies of 2 Hz, 5 Hz, and 10 Hz, respectively. Apart from the ability to function at high and low frequency, the proposed circuit also worked well with different types of PD (i.e. MFC and PVDF).

V. CONCLUSION

In this study, a DSHBR circuit for rectifying voltage and power from PEH system under high and low frequencies of vibrations and human motion-induced excitation was designed and investigated. By assimilating the advantage of MOSFETs, which has low threshold voltage in Stage – 1, and DC-DC converter, which stabilises the rectified voltage in Stage – 2, the DSHBR circuit successfully produced higher rectified voltage with fewer ripples and higher output power when compared with the regular H-Bridge circuit. In addition, the voltage rectified through the proposed circuit as a result of low frequency PEH was found to be able to charge a solar battery, demonstrating the practical application of the circuit. In the HMIV test involving arm movement, the proposed circuit delivered 3.4 V_{dc} of rectified voltage and 115.6 μW of output power from PVDF, while in the SIV tests, 8.8 V_{dc} and 84.2 μW of rectified voltage and output power was achieved. For future work, modification of the DSHBR circuit to incorporate the non-linear process is recommended.

REFERENCES

[1] M. Sedighi, R. V. Padilla, R. A. Taylor, M. Lake, I. Izadgoshasb, and A. Rose, "High-temperature, point-focus, pressurised gas-phase solar receivers: A comprehensive," *Energy Convers. Managemen*, vol. 185, pp. 678–717, Apr. 2019.

[2] S. Roundy, P. K. Wright, and J. Rabaey, "A study of low level vibrations as a power source for wireless sensor nodes," *Comput. Commun.*, vol. 26, no. 11, pp. 1131–1144, Jul. 2003.

[3] M. Sedighi, R. V. Padilla, P. Alamdari, M. Lake, A. Rose, I. Izadgoshasb, and R. A. Taylor, "A novel high-temperature (>700 °C), volumetric receiver with a packed bed of transparent and absorbing spheres," *Appl. Energy*, vol. 264, Apr. 2020, Art. no. 114705.

[4] I. Izadgoshasb, Y. Y. Lim, L. Tang, R. V. Padilla, Z. S. Tang, and M. Sedighi, "Improving efficiency of piezoelectric based energy harvesting from human motions using double pendulum system," *Energy Convers. Manage.*, vol. 184, pp. 559–570, Mar. 2019.

[5] Y. Y. Lim, S. T. Smith, R. V. Padilla, and C. K. Soh, "Monitoring of concrete curing using the electromechanical impedance technique: Review and path forward," *Struct. Health Monitor.*, vol. 20, no. 2, pp. 604–636, Mar. 2021.

[6] Y. Y. Lim, S. T. Smith, and C. K. Soh, "Wave propagation based monitoring of concrete curing using piezoelectric materials: Review and path forward," *NDT E Int.*, vol. 99, pp. 50–63, Oct. 2018.

[7] N. A. A. Nawir, A. A. Basari, M. S. M. Saat, N. X. Yan, and S. Hashimoto, "A review on piezoelectric energy harvester and its power conditioning circuit," *ARPN J.*, 2018.

[8] A. Rahman, O. Farrok, M. R. Islam, and W. Xu, "Recent progress in electrical generators for oceanic wave energy conversion," *IEEE Access*, vol. 8, pp. 138595–138615, 2020.

[9] A. S. Sadangi, S. K. Sahu, and K. Patra, "Comparison of circuits for dielectric elastomer based energy harvesting," in *Proc. 2nd Int. Conf. Inventive Syst. Control (ICISC)*, Jan. 2018, pp. 413–417.

[10] A. M. Eltamaly and K. E. Addoweesh, "A novel self-power SSHI circuit for piezoelectric energy harvester," *IEEE Trans. Power Electron.*, vol. 32, no. 10, pp. 7663–7673, Oct. 2017.

[11] S. Du, G. A. J. Amaratunga, and A. A. Seshia, "A cold-startup SSHI rectifier for piezoelectric energy harvesters with increased open-circuit voltage," *IEEE Trans. Power Electron.*, vol. 34, no. 1, pp. 263–274, Jan. 2019.

[12] M. Edla, Y. Y. Lim, M. Deguchi, R. V. Padilla, and I. Izadgoshasb, "An improved self-powered H-Bridge circuit for voltage rectification of piezoelectric energy harvesting system," *IEEE J. Electron Devices Soc.*, vol. 8, pp. 1050–1062, 2020.

[13] M. Edla, Y. Y. Lim, R. V. Padilla, and M. Deguchi, "An improved rectifier circuit for piezoelectric energy harvesting from human motion," *Appl. Sci.*, vol. 11, no. 5, p. 2008, Feb. 2021.

[14] M. Edla and Y. Y. Lim, "An improved piezoelectric energy harvesting circuit for reducing the internal loss," in *Proc. 83rd Researchfora Int. Conf.*, New Delhi, India, Jan. 2020, pp. 4–8.

[15] T. Kashiwao, I. Izadgoshasb, Y. Y. Lim, and M. Deguchi, "Optimization of rectifier circuits for a vibration energy harvesting system using a macro-fiber composite piezoelectric element," *Microelectron. J.*, vol. 54, pp. 109–115, Aug. 2016.

[16] S. Du, Y. Jia, C. Zhao, G. A. J. Amaratunga, and A. A. Seshia, "A nail-size piezoelectric energy harvesting system integrating a MEMS transducer and a CMOS SSHI circuit," *IEEE Sensors J.*, vol. 20, no. 1, pp. 277–285, Jan. 2020.

[17] F. Maiorca, F. Giusa, C. Trigona, B. Andò, A. R. Bulsara, and S. Baglio, "Diode-less mechanical H-bridge rectifier for zero threshold," vibration energy harvesters," *Sens. Actuators A, Phys.*, vol. 201, pp. 246–253, Oct. 2013.

[18] J. Colomer-Farrarons, P. Miribel-Catala, A. Saiz-Vela, M. Puig-Vidal, and J. Samitier, "Power-conditioning circuitry for a self-powered system based on micro PZT generators in a 0.13-μm low-voltage low-power technology," *IEEE Trans. Ind. Electron.*, vol. 55, no. 9, pp. 3249–3257, Sep. 2008.

[19] A. A. C. Asis and S. E. Rajan, "Efficiency evaluation of a MOSFET bridge rectifier for powering LEDs using piezo-electric energy harvesting systems," *Automatika*, vol. 57, no. 2, pp. 329–336, Jan. 2016.

[20] Y. Liu, G. Tian, Y. Wang, J. Lin, Q. Zhang, and H. F. Hofmann, "Active piezoelectric energy harvesting: General principle and experimental demonstration," *J. Intell. Mater. Syst. Struct.*, vol. 20, no. 5, pp. 575–585, Mar. 2009.

[21] K. Savarimuthu, R. Sankararajan, and S. Murugesan, "Design and implementation of piezoelectric energy harvesting circuit," *Circuit World*, vol. 43, no. 2, pp. 63–71, May 2017.

[22] J.-C. Hsieh and T.-H. Tsai, "An AC–DC wind energy harvesting circuit with extended input-voltage range and 95% tracking efficiency," in *Proc. IEEE Int. Symp. Circuits Syst. (ISCAS)*, May 2018, pp. 1–4.

[23] L. Wu, X.-D. Do, S.-G. Lee, and D. S. Ha, "A self-powered and optimal SSHI circuit integrated with an active rectifier for piezoelectric energy harvesting," *IEEE Trans. Circuits Syst. I, Reg. Papers*, vol. 64, no. 3, pp. 537–549, Mar. 2017.

[24] A. Tabesh and L. G. Frechette, "A low-power stand-alone adaptive circuit for harvesting energy from a piezoelectric micropower generator," *IEEE Trans. Ind. Electron.*, vol. 57, no. 3, pp. 840–849, Mar. 2010.

[25] S. Hashemi, M. Sawan, and Y. Savaria, "A novel low-drop CMOS active rectifier for RF-powered devices: Experimental results," *Microelectron. J.*, vol. 40, no. 11, pp. 1547–1554, Nov. 2009.

[26] G. K. Ottman, H. F. Hofmann, A. C. Bhatt, and G. A. Lesieutre, "Adaptive piezoelectric energy harvesting circuit for wireless remote power supply," *IEEE Trans. Power Electron.*, vol. 17, no. 5, pp. 669–676, Sep. 2002.

[27] Maxim. (Jun. 1, 2020). *High-Efficiency, Low-Supply-Current, Compact, Step-Up DC–DC Converters*. [Online]. Available: https://www.maximintegrated.com/en/products/power/switching-regulators/MAX1675.html

[28] E. Lefeuvre, D. Audigier, C. Richard, and D. Guyomar, "Buck-boost converter for sensorless power optimization of piezoelectric energy harvester," *IEEE Trans. Power Electron.*, vol. 22, no. 5, pp. 2018–2025, Sep. 2007.

[29] L. Yu, H. Wang, and A. Khaligh, "A discontinuous conduction mode single-stage step-up rectifier for low-voltage energy harvesting applications," *IEEE Trans. Power Electron.*, vol. 32, no. 8, pp. 6161–6169, Aug. 2017.

[30] H. Wang, Y. Tang, and A. Khaligh, "A bridgeless boost rectifier for low-voltage energy harvesting applications," *IEEE Trans. Power Electron.*, vol. 28, no. 11, pp. 5206–5214, Nov. 2013.

[31] M. H. Rashid, *Power Electronics Handbook*. Oxford, U.K.: Butterworth-Heinemann, 2017.

[32] V. Subramanyam, *Power Electronics-Devices, Converters and Applications*. Bangalore, India: New Age International Publishers, 2006.

[33] I. Izadgoshasb, Y. Lim, R. Vasquez Padilla, M. Sedighi, and J. Novak, "Performance enhancement of a multiresonant piezoelectric energy harvester for low frequency vibrations," *Energies*, vol. 12, no. 14, p. 2770, Jul. 2019.
[34] C. Peters, O. Kessling, F. Henrici, M. Ortmanns, and Y. Manoli, "CMOS integrated highly efficient full wave rectifier," in *Proc. IEEE Int. Symp. Circuits Syst.*, May 2007, pp. 2415–2418.

MAHESH EDLA was born in India, in 1993. He received the B.Tech. degree in electrical and electronics engineering from JNTUH, India, and the M.Sc. degree in electrical and electronics engineering from Coventry University, U.K. He is currently pursuing the Ph.D. degree in electronics engineering with Southern Cross University, Australia. He worked with Coventry University in the field of piezoelectric energy harvesting for four months. He is currently a Contract Lecturer with the School of Engineering, Southern Cross University. His current research interest includes designing electronic circuits for the rectification process.

YEE YAN LIM received the Ph.D. degree in civil engineering from Nanyang Technological University, Singapore, in 2012. He is currently a Senior Lecturer and a Civil Engineering Course Coordinator with the School of Environment, Science and Engineering, Southern Cross University. His current research interests include smart materials based structural health monitoring and energy harvesting.

RICARDO VASQUEZ PADILLA received the B.S. and M.Sc. degrees in mechanical engineering, and the Ph.D. degree from the Department of Chemical and Biomedical Engineering, University of South Florida, in 2011. From 2011 to 2014, he was an Assistant Professor with Universidad Del Norte. From 2014 to 2016, he worked as a Research Fellow with the CSIRO Energy Centre at Newcastle. He is currently a Senior Lecturer and a Course Coordinator of Bachelor in Mechanical Engineering with the School of Environment, Science and Engineering, Southern Cross University. He is also working on the design of solar gas phase receivers and self-tunable wind energy harvesters. His research interests include modeling, optimization, mechanical design, economic analysis, and testing of thermo-mechanical systems.

DEGUCHI MIKIO received the master's degree from the Graduate School of Engineering, Kyoto University, in 1985, and the Ph.D. degree in engineering from Kyoto University, in 2003. After working at Mitsubishi Electric Corporation for about ten years, he was transferred to the Niihama College, National Institute of Technology (KOSEN), where he is currently a Professor with the Department of Electronics and Control Engineering. His research interests include electronic measurement technology, electronic circuit application, and development of intelligent teaching materials.